The Astrophysical Journal, 585:1147–1157, 2003 March 10

ELECTRON PROPERTIES AND COULOMB COLLISIONS IN THE SOLAR WIND AT 1 AU: *WIND* OBSERVATIONS

C. Salem,[1] D. Hubert,[2] C. Lacombe,[2] S. D. Bale,[1] A. Mangeney,[2] D. E. Larson,[1] and R. P. Lin[1]

Received 2002 October 31; accepted 2002 November 18

ABSTRACT

The question of what controls the electron properties in the solar wind has been the subject of several extensive analyses over the past 20 years. We analyze here the electron properties of the solar wind observed by the *Wind* satellite at 1 AU in the ecliptic plane, during 50 days close to the last minimum of solar activity. The electron temperature anisotropy $T_{e\parallel}/T_{e\perp}$, which seems to depend on the wind speed $V_{\rm sw}$, the density N_p, the heliomagnetic latitude λ_m, or the time, actually depends mainly on the Coulomb collisions. The collisional age A_e is the number of transverse collisions suffered by a thermal electron during the expansion of the wind over the scale of the density gradient. The A_e depends on $V_{\rm sw}$, on N_p, and thus on λ_m; it also depends on the time because it changes strongly at the crossing of a stream interface. We show that $T_{e\parallel}/T_{e\perp}$ is strongly correlated with $1/A_e$. The effect of Coulomb collisions on the electron heat flux are also investigated. We find that the total electron heat flux Q_e displays an upper bound that is inversely proportional to the collisional age, in favor of a regulation of the heat flux by Coulomb collisions. The observed heat flux is then compared to the collisional heat flux of the classical Spitzer-Härm (SH) theory. Although earlier observations have shown that the electron heat flux in the solar wind at 1 AU is well below the values given by the SH theory, we find that the observed heat flux reaches the SH limit for the lowest values of the electron mean free paths. The Coulomb collisions thus seem to play a part in the regulation of the electron heat flux in the solar wind.

Subject headings: methods: data analysis — plasmas — solar wind

1. INTRODUCTION

One of the major issues of solar wind physics that is still not fully understood concerns the radial evolution of solar wind internal energy. This fundamental issue is related to the more general problem of the transport of heat through a weakly collisional plasma, beyond the framework of heliospheric physics. Because of their low mass, the electrons play an important role in the solar wind expansion and the associated energy transport since they are the dominant carriers of the total heat flux. Indeed, the electron heat flux is believed to be one of the energy sources that drives the expansion of the solar corona (Hundhausen 1972; Feldman et al. 1975; Marsch 1991). As a result of low collision rates in the solar wind, the electrons develop temperature anisotropies and their velocity distribution functions (VDFs) become skewed and develop tails and heat fluxes along the local magnetic field direction. However, these nonthermal characteristic of the VDFs are not as strong as predicted by collisionless (or exospheric) models (Jockers 1970; Lemaire & Scherer 1971), implying that some microphysical processes (Coulomb collisions and/or wave-particle inter actions) must act locally to control or regulate these anisotropies.

This fundamental problem has motivated more than 20 years of studies of the properties of electrons in the solar wind, and the solar wind parameters on which these properties depend, at a given distance from the Sun. First, we summarize the main results from previous observations. These observations concern essentially the electron temperature T_e, the temperature anisotropy $T_{e\parallel}/T_{e\perp}$, the heat flux, and the solar wind parameters that control them. Here $T_{e\parallel}/T_{e\perp}$ is the ratio of the electron temperature, in a direction parallel to the background magnetic field B, over the temperature perpendicular to B. We consider only the global electron properties, without distinguishing between the core, the halo, and the strahl of the velocity distribution function.

Using *Interplanetary Monitoring Platform 6*, *7*, and *8* data, Feldman et al. (1975) showed that in the ecliptic plane, $T_{e\parallel}/T_{e\perp}$ is larger in the fast wind than in the slow wind. With *ISEE 3* data, Phillips et al. (1989) found that $T_{e\parallel}/T_{e\perp}$ increases when the wind speed $V_{\rm sw}$ increases and when the proton density N_p decreases; this dependence on the speed and on the density indicated that the Coulomb collisions play a part in the solar wind. *Helios* observations, still in the ecliptic plane (Pilipp et al. 1987c, 1990), showed the following (1) The electron temperature T_e is minimum and isotropic at the boundary between the magnetic sectors, the heliospheric current sheet (HCS); T_e is stronger and anisotropic before and after the HCS crossings; and it is weaker and more anisotropic far from the HCS, in the fast wind. (2) The heat flux Q_e is often minimum at the HCS and maximum in the compression regions; the normalized heat flux is minimum at the HCS, maximum far from the HCS. (3) The strahl (beam of electrons with an energy larger than about 100 eV) is measured within a narrow angle around the B direction in the fast wind; this angle is broader near the HCS; and there is no strahl at the HCS. Pilipp et al. (1987c) concluded that the electron properties depend on the distance from the HCS more than on the wind speed.

This conclusion was only partly confirmed by the *Ulysses* observations out of the ecliptic. Phillips et al. (1995) found that T_e tends to decrease poleward and that $T_{e\parallel}/T_{e\perp}$ increases slightly with the heliographic latitude λ_g (and thus probably with the heliomagnetic latitude λ_m, which is the

[1] Space Sciences Laboratory, University of California, Berkeley, CA 94720; salem@ssl.berkeley.edu.

[2] Laboratoire d'Etudes Spatiales et d'Instrumentation en Astrophysique, Observatoire de Paris, F-92195 Meudon, France.

latitude with respect to the HCS). However, Scime et al. (1995, 2001) and Scime, Badeau, & Littleton (1999) did not find a significant variation of Q_e with λ_g. Hammond et al. (1996) concluded that neither Q_e nor the strahl depends on λ_g. Furthermore, Scime et al. (2001) did not find a significant correlation between the magnitude of the electron heat flux and the solar wind speed, during both solar minimum and solar maximum.

In the ecliptic plane, Fitzenreiter et al. (1998) observed on *Wind* that the flux of the strahl is more intense, and the strahl angle more narrow, in the fastest wind. As did Feldman et al. (1975), Fitzenreiter et al. (1998) thus found that the wind speed is the main parameter that controls the electron anisotropy and the strahl properties. Ogilvie et al. (1999) observed the strahl properties before and after the crossing of the stream interface (SI) between the slow wind and the fast wind. At the SI, the wind speed V_{sw} and the proton temperature T_p increase and N_p decreases; generally, a spacecraft at 1 AU crosses an SI after the HCS (Gosling et al. 1978). Ogilvie et al. (1999) found that the flux of the strahl was minimum before the SI and maximum after.

Following these observations, the parameters controlling the electron temperature T_e, the temperature anisotropy $T_{e\parallel}/T_{e\perp}$, and the heat flux Q_e can thus be the wind speed V_{sw}, the density N_e (and thus the Coulomb collision frequency), the heliomagnetic latitude λ_m, or even the time (before or after the SI). These dependences give some clues as to the relative importance of the processes that play roles in determining solar wind electron dynamics, such as Coulomb collisions or wave-particle interactions, but also the large-scale interplanetary electrostatic potential and magnetic field (Marsch 1991). However, to date, our understanding of what controls the solar wind electron properties is still far from being complete.

In this paper, we investigate the above dependences using data from the *Wind* spacecraft. First, we consider how $T_{e\parallel}/T_{e\perp}$ depends on V_{sw}, N_e, λ_m, or the time (before and after an SI), parameters that are not independent. We confirm qualitatively the dominant role of the collision number in controlling the temperature anisotropies. The effect of Coulomb collisions on the electron heat flux Q_e is also investigated. It is well known (see Scime et al. 1994a) that the heat flux Q_e observed in the solar wind is weaker than the collisional heat flux due to the thermal conductivity calculated by Spitzer & Härm (1953). Thus, based on this fact, the role of the collisions in controlling the electron heat flux has always been argued to be negligible. However, to illustrate that collisions may play at least a small part in the regulation of the heat flux, we show that the upper bound of the total electron heat flux is inversely proportional to the collision frequency. Moreover, the observed heat flux appears to reach the Spitzer-Härm limit for the smallest values of the collisional mean free path in the solar wind.

Before analyzing the parameters that control the electron properties, let us recall what controls the proton properties in the solar wind: (1) The speed V_{sw}, the temperature T_p, and the density N_p mainly depend on the heliomagnetic latitude λ_m (Bruno et al. 1986; Lacombe et al. 2000). This implies that the protons at 1 AU remember the initial conditions close to the Sun, which themselves depend on the latitude, as in the model of Pizzo (1994). (2) The total pressure P (magnetic plus thermal) in the solar wind is an important parameter for the proton properties: the latitudinal dependences of V_{sw}, T_p, and $|B|$ are not the same in the low-pressure wind ($P \leq 5 \times 10^{-11}$ Pa) and in the high-pressure wind (Lacombe et al. 2000). (3) The proton properties are time dependent: at the same latitude λ_m, they are not the same before and after the HCS crossing (Borrini et al. 1981; Lacombe et al. 2000). These two last dependences show the part played by the dynamical interactions, between the Sun and 1 AU, which reduce the effects of the initial conditions on the proton properties. In our study, we sometimes consider separately the low-pressure wind, in which there are fewer local and temporal variations masking the overall dependences of the electron properties on the solar wind expansion.

2. INSTRUMENTS AND DATA

The *Wind* spacecraft, launched on 1994 November 1, was designed to observe the solar wind approaching Earth from a position near Lagrange point L1. *Wind* is equipped with state-of-the-art instruments to measure three-dimensional electron and ion distribution functions, and plasma waves, as well as magnetic field. We use data from the Three-Dimensional Particle (3DP; Lin et al. 1995) and Waves (Bougeret et al. 1995) experiments, as well as spin resolution (3 s) magnetic field data from the Magnetic Field Investigation (MFI) experiment (Lepping et al. 1995), all on the *Wind* spacecraft.

The 3DP experiment is designed to make measurements of the full three-dimensional distributions of electrons and protons from energies of the order of those of the thermal solar wind plasma to those of low-energy cosmic rays, with a high-sensitivity, wide dynamic range, good energy and angular resolution, and high time resolution. The solar wind energy range for both electrons and protons is well covered by EESA-L and PESA-L, respectively, one of the pairs of electron and proton electrostatic analyzers (EESAs and PESAs). In normal modes of operation, the EESA-L analyzer measures the electron velocity distribution functions (VDFs) from a few eV to 1.1 keV (energy resolution of $\sim$20%) with 15 logarithmically spaced energy steps and full 4π angular coverage in one spacecraft rotation ($\sim$3 s). Because of the allowed telemetry rate, the full three-dimensional VDFs are transmitted only every $\sim$99 s (for the time period considered in this paper). However, onboard computed moments of the VDFs (density, velocity, pressure, temperature, and heat flux) are transmitted routinely every 3 s.

It is important to emphasize here the relative difficulty in measuring electron VDFs in the solar wind, where such measurements are in general drastically affected by spacecraft charging effects. The spacecraft charging effects severely pollute and distort the electron VDFs at low energies (in the thermal range) by modifying both the energies and direction of motion of the solar wind electrons incident on the detector (e.g., Scime, Phillips, & Bame 1994b; Salem et al. 2001). These effects generally combine with other instrumental effects such as the incomplete sampling of the VDFs due to a nonzero low-energy threshold of the energy sweeping in the electron spectrometer (Song, Zhang, & Paschmann 1997; Salem et al. 2001). Consequently, all the moments of the VDFs are severely affected as well (see Salem et al. 2001 and references therein). Accurate measurements of the solar wind electron parameters require therefore a full correction of these effects. This correction is generally not quite straightforward to carry out since the

spacecraft electric potential is often an unknown parameter that depends on the electron density and temperature that one wishes to measure.

The question of the accuracy of the electron measurements on the *Wind* spacecraft has recently been addressed by Salem et al. (2001). They developed a new method to determine accurate solar wind electron density and temperature using the data of a particle detector and a plasma wave receiver. Through a simple scalar correction model, they established the correction equations for the electron density and temperature approximating the actual solar wind electron VDF by an isotropic Maxwellian. The electron density data determined from the wave receiver Thermal Noise Receiver (TNR) of the Waves experiment, taken as a reference, is used as an alternative to the use of approximate values for the spacecraft potential. This determination of the electron density relies on the identification of the "plasma line" at the local electron plasma frequency in the spectrum of the thermal noise (Salem 2000; Salem et al. 2001) and is quite immune to the spacecraft charging effects (Meyer-Vernet et al. 1998; Issautier et al. 1999).

In this study, we use the TNR electron density N_e, determined at a resolution of 4.5 s, and the 3DP solar wind velocity $V_{\rm sw}$ and proton temperature T_p calculated on board from the PESA-L ion electrostatic analyzer every 3 s. We use Salem's model to calculate the electron temperature from the raw 3DP electron temperature calculated on board at a resolution of 3 s (using eq. [24] in Salem et al. 2001). This corrected 3DP electron temperature is on average 4 eV lower than the raw temperature, their relative difference being 35% on average. The determination of any parameter that depends on the electron temperature can be biased by such a difference, and thus the interpretation of the results. On average, the corrected 3DP electron temperature is found to lie around 12.1 ± 3.1 eV, which is in very good agreement with earlier results near 1 AU (see Feldman et al. 1975; Newbury et al. 1998). We also use the detailed electron distribution functions measured by the 3DP from the energy threshold $E_{\rm min} = 9.65$ eV up to about 1.1 keV. We integrated these electron distribution functions to calculate the ratio $T_{e\parallel}/T_{e\perp}$ (using the magnetic field data from the MFI experiment) and the electron heat flux vector every 1.5 minutes. We assume here that the effect of the spacecraft potential is isotropic so that, as a first order, the ratio $T_{e\parallel}/T_{e\perp}$ is not affected. The electron heat flux, the third moment of the electron velocity distribution function, has been calculated by replacing the bulk electron velocity by the bulk proton velocity: as shown by Salem et al. (2001), the heat flux vector is then found statistically aligned with the magnetic field, while it was found 20° eastward when calculated in the electron frame.

The data presented in this paper are taken from the first *Wind* apogee pass near L1, in 1995, where the spacecraft spent several months following a series of phasing orbits. The chosen time interval is close to the last solar cycle minimum. It extends from 1995 May 15 to July 3, i.e., from 135.0 to 185.0 decimal days of the year. Until July 3, *Wind* was around the Lagrange point, at 200 Earth radii ($R_\oplus$) or more from the Earth. This interval was selected because no transient magnetic cloud or strong interplanetary shock was observed during these 50 days (Sanderson et al. 1998), so the analyzed properties are those of the ambient solar wind. All the data sets and the calculated quantities have been smoothed and resampled to give only 125 points per day (averages over about 10 minutes). From day 157.6 to 161.6, there are frequent and large data gaps in the electron distribution functions, so the calculated averages of the electron heat flux can be biased.

To determine the heliomagnetic latitude λ_m of *Wind*, we have to make hypotheses about the position of the HCS during the considered interval. The position of the HCS has been deduced from the classic model of Hoeksema, Wilcox, & Scherrer (1983; available on line) and improved by the *Wind* observations of the current sheet crossings and of the direction of the total electron heat flux (Lacombe et al. 2000).

The thin line in Figure 1*a* is a plot of λ_m as a function of time in days; $\lambda_m = 0$ corresponds to the HCS crossings. Because the solar wind proton properties depend not only on $|\lambda_m|$ but also on the time (before or after the HCS crossings), we have also considered a *superposed epoch latitude* $\lambda_{\rm se}$ (Lacombe et al. 2000), which has the same modulus $|\lambda_{\rm se}| = |\lambda_m|$ but is taken as negative before the closest HCS crossing and positive after. This definition of $\lambda_{\rm se}$ is illustrated in Figure 2, and $\lambda_{\rm se}$ is shown as the thick line in

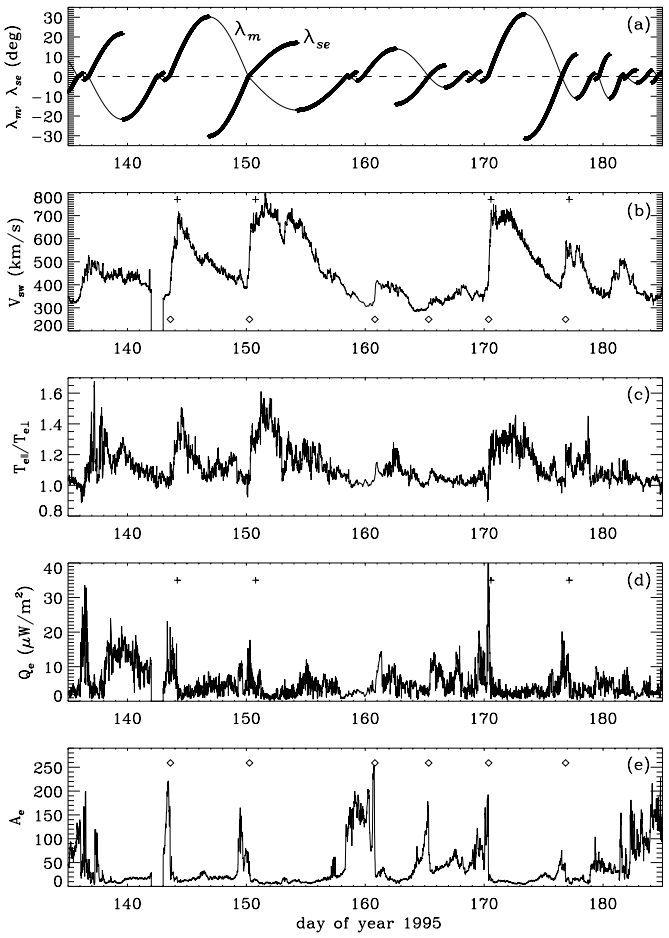

FIG. 1.—Fifty consecutive days of data in 1995 (from May 15 to July 3). (*a*) Latitude of *Wind* with respect to the magnetic sector boundary or HCS: λ_m (*thin line*) is Hoeksema's estimation, adjusted with HCS crossings observed on *Wind* (§ 2), and $\lambda_{\rm se}$ is the superposed epoch latitude defined in Fig. 2. (*b*) Wind speed in km s^{-1}. (*c*) Electron temperature anisotropy. (*d*) Total electron heat flux in μW m^{-2}. (*e*) Electron collisional age (eq. [6] in § 4). The plus signs at the top of (*b*) and (*d*) indicate the crossings of four weak reverse interplanetary shocks, and the diamonds on (*b*) and (*e*) indicate the crossings of six SIs.

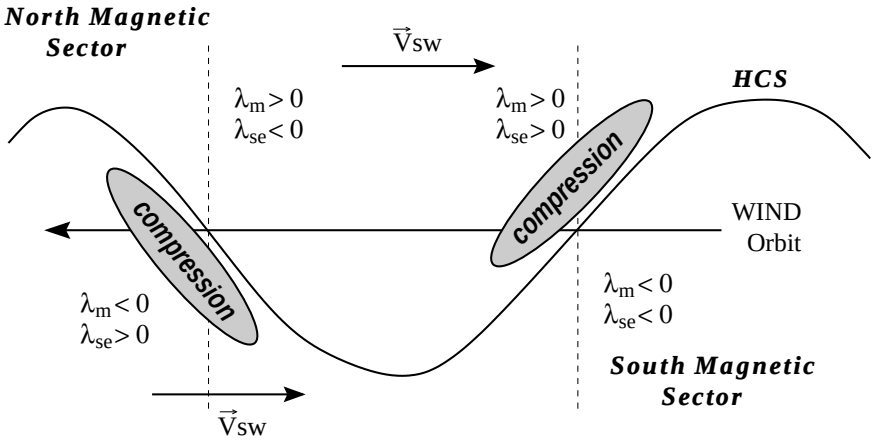

FIG. 2.—Schematic definition of the superposed epoch latitude λ_{se} in comparison to the heliomagnetic latitude λ_m

Figure 1*a*. The solar wind speed is displayed in Figure 1*b*. The temperature anisotropy $T_{e\parallel}/T_{e\perp}$ is given in Figure 1*c*, and the modulus Q_e of the electron heat flux vector in Figure 1*d*. The plus signs at the top of Figures 1*b* and 1*d* indicate the crossings of four weak reverse interplanetary shocks; the diamonds in Figures 1*b* and 1*e* indicate the crossings of six regions that are probably SIs. Figure 1*e* will be discussed in § 4.

3. ROLE OF THE LATITUDE

As explained in the introduction, the heliomagnetic latitude has long been considered to be the parameter that best organizes the solar wind electron properties (Pilipp et al. 1987a, 1987c), as is actually the case for the proton properties (Bruno et al. 1986; Lacombe et al. 2000). In Figure 3, we display the electron properties (namely, the electron temperature T_e, the electron temperature anisotropies $T_{e\parallel}/T_{e\perp}$, the total electron heat flux Q_e, and the normalized heat flux Q_n) as functions of the superposed epoch heliomagnetic latitude λ_{se}, for the low-pressure solar wind ($P \leq P_c$; left panels of Fig. 3) and the high-pressure wind ($P > P_c$; right panels of Fig. 3). The considered pressure is the total pressure (thermal + magnetic),

$$P = N_e k_B (T_e + T_p) + \frac{B^2}{2\mu_0} , \quad (1)$$

and the critical value is $P_c \simeq 6.4 \times 10^{-11}$ Pa. The normalized heat flux is defined by

$$Q_n = Q_e / Q_0 , \quad (2)$$

where Q_0, given by

$$Q_0 = \tfrac{3}{2} N_e k_B T_e v_{the} , \quad (3)$$

is the *free-streaming heat flux*, which is a "saturation" level for the heat flux (Hundhausen 1972), defined as the heat flux obtained if the internal energy of the distribution, $\frac{3}{2} N_e k_B T_e$, were convected at the thermal speed of the electrons v_{the},

$$v_{the} = \sqrt{\frac{2 k_B T_e}{m_e}} . \quad (4)$$

This normalization by the free-streaming heat flux is widely used in the literature (see for instance Hundhausen 1972; Feldman et al. 1975; Pilipp et al. 1987a; Gary et al. 1994, 1999). It is justified by the fact that internal energy cannot be transported by thermal motions at a rate greater than (or probably even as large as) Q_0 (Parker 1964). Q_n can also be seen as a measure for the skewing of the distribution functions (Pilipp et al. 1987a).

Following Figure 3, some of the observations of Pilipp et al. (1987c, 1990) are confirmed; other observations are not confirmed. For instance, we confirm that T_e is larger, on average, at $|\lambda_{se}| \simeq 15°$ than at $|\lambda_{se}| \simeq 25°$; but this is true only in the low-pressure wind (see Figs. 3*a* and 3*b*). We confirm that the weakest values of T_e (≤ 8 eV) are observed at the HCS, whatever the pressure is; but T_e can also reach 15–20 eV at the HCS. We confirm that $T_{e\parallel}/T_{e\perp}$ is weaker, on average, at low latitudes. However, Figures 3*c* and 3*d* mainly show that the distribution of $T_{e\parallel}/T_{e\perp}$ is different before the crossing of the HCS ($\lambda_{se} < 0$) and after the HCS ($\lambda_{se} > 0$). Because the SI generally occurs just after the HCS, this asymmetry can be compared with the asymmetry observed by Ogilvie et al. (1999) for the strahl, before and after the SI. As for the heat flux, we confirm that the total heat flux Q_e is maximum in the compression regions (see Fig. 3*f*) but does not depend on the latitude (Fig. 3*e*). The normalized heat flux Q_n is weaker, on average, at low latitudes, especially in the compressed regions (see Fig. 3*h*), but this is less clear for the low pressures (Fig. 3*g*), where a peak of Q_n is observed.

From Figure 3, we can conclude that the correlation between the electron properties and the angular distance $|\lambda_{se}| = |\lambda_m|$ from the HCS is not so strong. We have to look for correlations of $T_{e\parallel}/T_{e\perp}$ with other solar wind parameters.

4. ROLE OF THE COLLISIONS

In this section, we focus our analysis on the temperature anisotropy $T_{e\parallel}/T_{e\perp}$. Figures 4*a*–4*d* display $T_{e\parallel}/T_{e\perp}$ as a function of $|\lambda_m|$, V_{sw}, N_p, and T_e. We can see that the correlation with V_{sw} is better than the correlation with $|\lambda_m|$, and the best correlation is with $1/N_p$. These good correlations, already observed by Phillips et al. (1989), have shown the importance of the Coulomb collisions suffered by the thermal electrons.

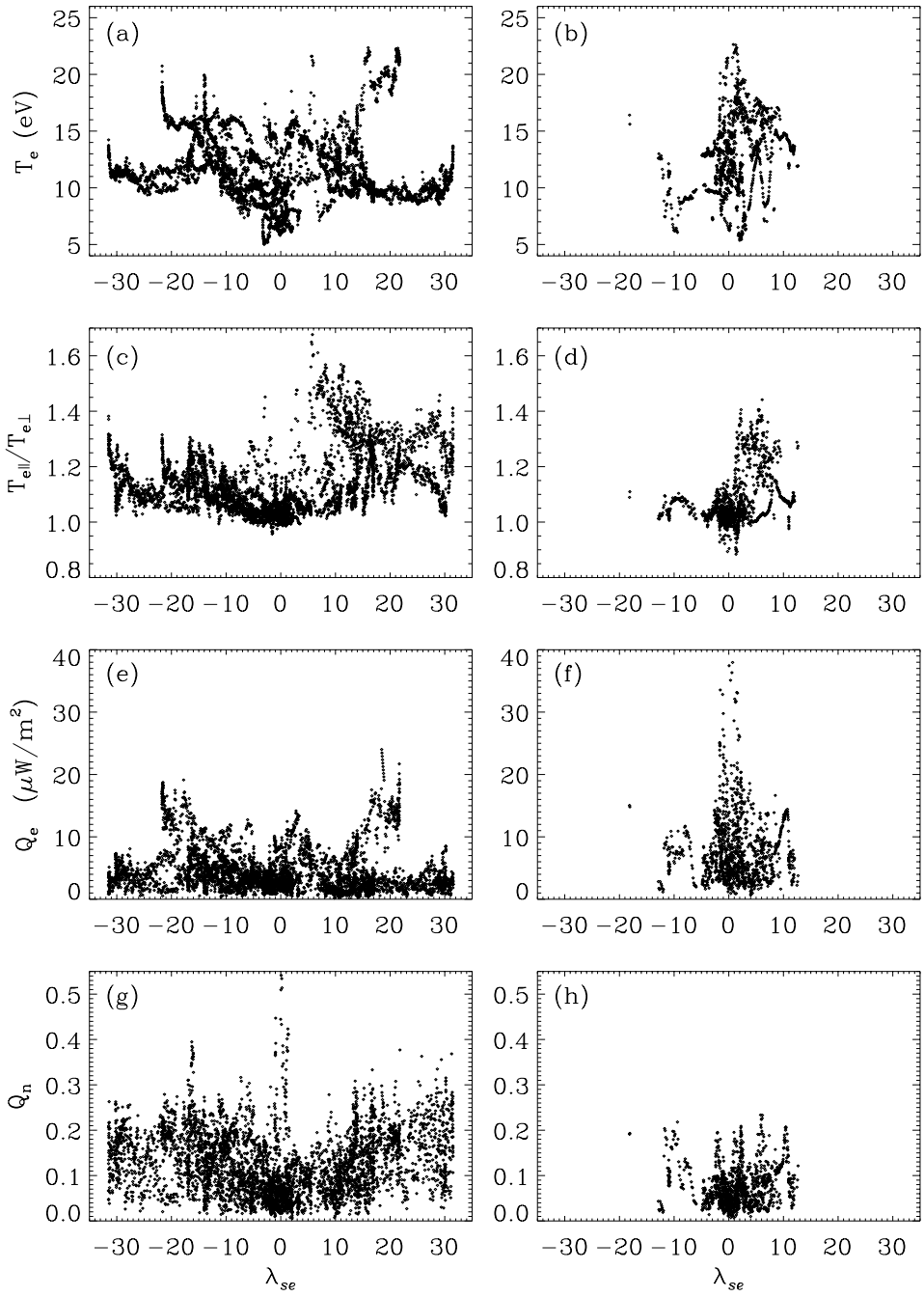

FIG. 3.—Fifty consecutive days. Scatter plots of 11 minute averages (125 points day^{-1}) of the electron temperature T_e, the electron temperature anisotropy $T_{e\parallel}/T_{e\perp}$, the total electron heat flux Q_e, and the normalized heat flux Q_n (eq. [2]), in a low-pressure wind (*left panels*) and in a compressed wind (*right panels*) as a function of λ_m. The critical pressure separating both wind regimes is $P_c = P_{\mathrm{Th}+M} = 6.4 \times 10^{-11}$ Pa.

How do we calculate the collision number? Let us consider the *e*-*e* collisions between thermal electrons, which produce a transverse diffusion. The collision frequency is

$$\nu_{e\perp} \simeq 7.710^{-6} N_e T_e^{-3/2} \ln \Lambda \, , \tag{5}$$

where T_e is in eV and N_e in cm^{-3}, and the so-called Coulomb logarithm $\ln \Lambda \simeq 25.5$ (see Spitzer 1956; Huda 2000). Following Phillips & Gosling (1990), if we add to the *e*-*e* collisions the *e*-*p* and *e*-α collisions with protons and α-particles, the total transverse collision frequency for a thermal electron in the solar wind is $\simeq 2.55\nu_{e\perp}$. Then, we integrate the number of collisions suffered by a thermal electron during the time of expansion of the solar wind over the scale of the density gradient, i.e., from $r = 0.5$ AU to $r = 1$ AU. We assume that V_{sw} is constant and that N_e and T_e vary with the distance as r^{-2} and $r^{-\alpha}$, respectively. This integral is then

$$A_e = 2.55\nu_{e\perp} \frac{R}{V_{\mathrm{sw}}} \left(\frac{2^{1-1.5\alpha} - 1}{1 - 1.5\alpha} \right) , \tag{6}$$

where $R = 1$ AU is in kilometers and V_{sw} in kilometers per second.

The value of α depends on the electron population (core or halo) and also on the wind regime (slow or fast wind). In

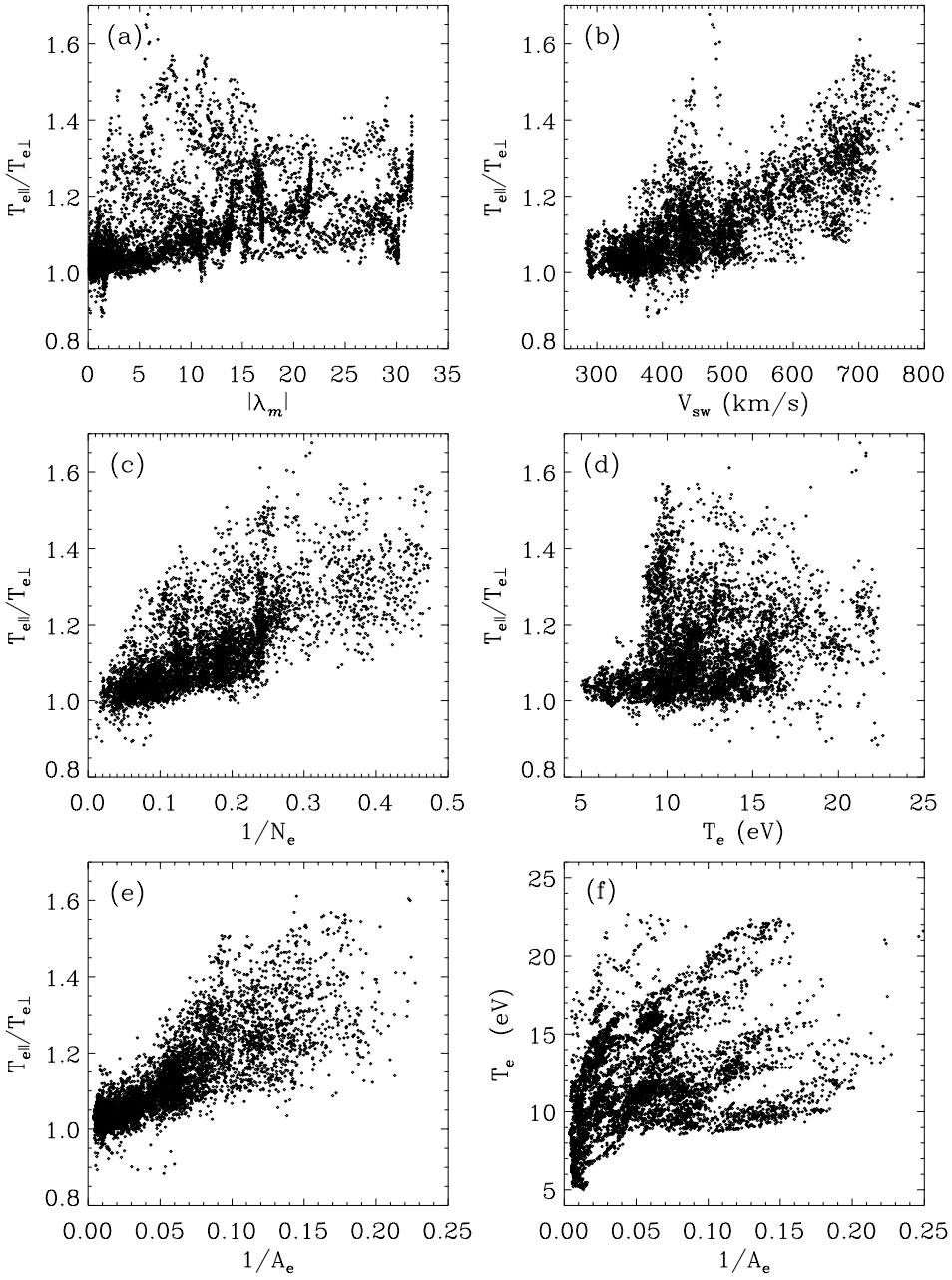

FIG. 4.—Fifty consecutive days. Scatter plots of 11 minute averages of the electron temperature anisotropy as a function of (*a*) heliomagnetic latitude $|\lambda_m|$, (*b*) wind speed V_{sw}, (*c*) inverse of the electron density, $1/N_e$, (*d*) electron temperature, T_e, and (*e*) the inverse of the collisional age, $1/A_e$. (*f*) Electron temperature as a function of the inverse of the collisional age.

the fast wind, *Ulysses* observations have shown that $\alpha \sim 0.6$ for the core electrons (Issautier et al. 1998) and $\alpha \sim 0.3$ for the halo electrons (Maksimovic, Gary, & Skoug 2000), so the total temperature T_e varies as $\sim r^{-0.5}$. As for the slow wind, T_e in the coronal streamers (sources of the slow wind) is known to be comparable to T_e in the coronal holes (sources of the fast wind), while T_e at 1 AU is considered to be higher in the slow wind than in the fast wind: T_e can then be considered to vary as $\sim r^{-0.4}$ in the slow wind (David et al. 1998; Fludra et al. 1999; Gibson et al. 1999). Since the time interval considered in this study mixes slow and fast winds, we decide to take an intermediate value for α, $\alpha \sim 0.45$.

The *collisional age* A_e (for $\alpha = 0.45$) as a function of time is displayed in Figure 1*e* and varies between 2 and 250 collisions; we see that A_e drops at the SI crossings indicated by diamonds.

Figure 4*e* shows that the correlation between $T_{e\parallel}/T_{e\perp}$ and $1/A_e$ is good: the anisotropy is weak for *collisionally old* plasmas (with large values of A_e) and stronger for *collisionally young* plasmas (with small values of A_e). There is an anticorrelation between A_e and $|\lambda_m|$: this is the reason why the part played by $|\lambda_m|$ was considered as dominant. Figure 4*e* thus shows qualitatively the control of $T_{e\parallel}/T_{e\perp}$ by the collisions.

The value of T_e is not correlated to $1/A_e$ (Fig. 4*f*): even if the lowest values of T_e ($\leq$8 eV) are found in a collisionally old plasma ($A_e > 20$), the same old plasma can have $T_e \simeq 16$ eV. This shows that the electron temperature T_e in

the slow solar wind displays a higher variability than in the fast wind, which is collisionally younger. Phillips & Gosling (1990) proposed a model in which $T_{e\parallel}$ and $T_{e\perp}$ evolve adiabatically in a collisional plasma with a spiral magnetic field. This model predicts a ratio $T_{e\parallel}/T_{e\perp}$ that is larger in the fast wind, as observed in our data (see Fig. 4*b*). It also predicts that the lowest values of T_e will be observed for the smallest ratios $T_{e\parallel}/T_{e\perp}$ because, in a marginally collisional plasma, the expansive cooling rate is smaller if temperature anisotropies are allowed to develop; this relation is also observed in our data (see Fig. 4*d*). However, some of the predictions of the model of Phillips & Gosling (1990), at large distance and large λ_g, have not been confirmed by the *Ulysses* observations. The model of Phillips & Gosling (1990) does not take into account the electron heat flux, which is observed in the solar wind, and the interplanetary electrostatic field, for which there is some observational evidence (Mangeney et al. 1999; Lacombe et al. 2002).

5. THE ELECTRON HEAT FLUX

A complete theory of the solar wind requires a thorough understanding of how Q_e evolves and how it is regulated during the solar wind expansion. We look here for relations between the solar wind properties and the electron heat flux Q_e and/or the normalized heat flux Q_n (eq. [2]).

5.1. *Low- and High-Pressure Wind Regimes*

We have shown in § 3 that there is no dependence of the electron heat flux on heliomagnetic latitude. This is in good agreement with *Ulysses* observations (Scime et al. 1995). However, the properties of the heat flux in the compressed regions are different from those in the ambient solar wind. This can be seen in Figure 5, which displays the total heat flux as a function of the total pressure (magnetic + kinetic). This scatter plot clearly shows two different branches for the heat flux: a narrow one for $P < P_c$, characterizing the low-pressure wind regime, and a more scattered one for $P > P_c$, characterizing the compressed regions, $P_c = 6.4 \times 10^{-11}$ Pa being the critical pressure separating both regimes (see § 3). Therefore, it is important to distinguish between both regimes when analyzing the properties of the electron heat flux. Hereafter, we consider only the low-pressure wind, unless stated, since we look for general trends in the regulation of the electron heat flux in the ambient solar wind.

The determination of the electron heat flux in the ambient solar wind can also be biased by the presence on some occasions of double-strahl electron distributions (see for instance Pilipp et al. 1987b) due to backstreaming suprathermal electrons. This can happen near 1 AU when the spacecraft is in the foreshock of the Earth's bow shock. We have thus systematically withdrawn the time intervals during which *Wind* is in the foreshock, i.e., downstream of a field line tangent to the bow shock, or during which *Wind* is upstream of this field line but at less than 50 $R_\oplus$ (along the geocentric solar ecliptic x-axis) of the foreshock boundary. Only 5% of our data set has thus been removed, corresponding to a geometry in which the interplanetary magnetic field is nearly radial because *Wind* was close to Lagrange point L1, at more than 200 $R_\oplus$ from the Earth.

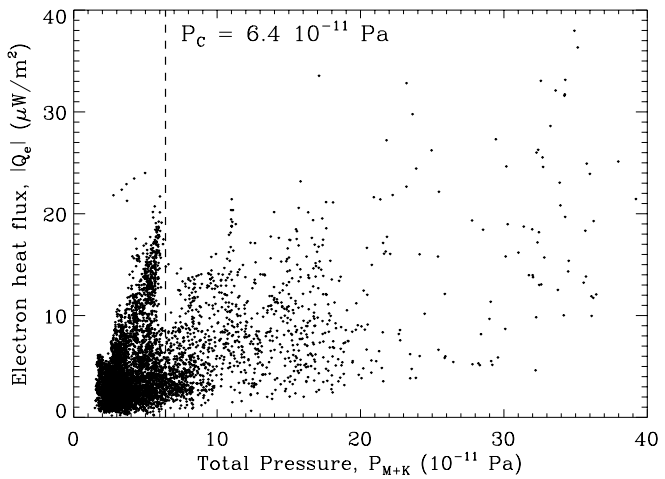

FIG. 5.—Fifty consecutive days. Scatter plot of 11 minute averages of the total electron heat flux Q_e as a function of the total pressure P_{Th+M} (eq. [1]). The vertical dashed line indicates the critical pressure $P_c = 6.4 \times 10^{-11}$.

5.2. *Relation between Heat Flux and Solar Wind Parameters*

In Figure 6, we display the electron heat flux Q_e (Fig. 6*a*) and the normalized heat flux Q_n (Fig. 6*b*) as functions of the wind speed V_{sw}, in the low-pressure and "free" solar wind

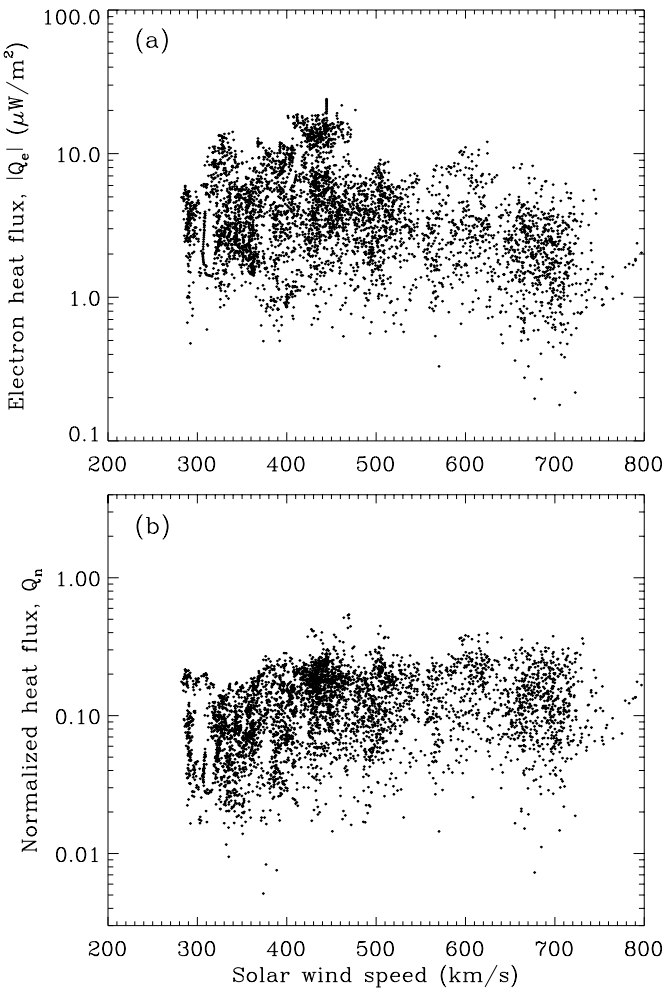

FIG. 6.—Fifty consecutive days. Scatter plots of 11 minute averages of (*a*) the total electron heat flux Q_e and (*b*) the normalized heat flux Q_n (eq. [2]) as functions of the solar wind speed V_{sw}, in the low-pressure and free solar wind (i.e., not connected to the Earth's bow shock).

(not connected to the Earth's bow shock). From this figure, we can conclude that there is no clear relation between Q_e (or Q_n) and the wind speed V_{sw}; this was also shown by Figure 3*a* of Scime et al. (2001), with a large data sample (over a whole solar cycle) from the *Ulysses* spacecraft. As pointed out by Scime et al. (2001), such a relation is predicted by models of a regulation of the solar wind electron heat flux by the interplanetary electrostatic potential (Hollweg 1974; Scudder & Olbert 1979a, 1979b). Some of these models predict that V_{sw} should be locally anticorrelated to Q_e (Scudder & Olbert 1979a, 1979b). On the other hand, other models suggest that both parameters should be correlated, since the presence of suprathermal tail in the electron distributions is expected to increase the solar wind speed (Maksimovic, Pierrard, & Lemaire 1997; Meyer-Vernet 1999): the more significant the tail (so the greater the heat flux), the larger the ambipolar electric field that then drives higher solar wind speeds. In any case, the absence of a relationship between the electron heat flux and the solar wind speed is an important piece of information, which suggests that the interplanetary potential is unlikely to play a significant role in the heat flux regulation as well as in the value of the solar wind velocity at 1 AU.

On the other hand, the electron heat flux appears to be related to the collision frequency. In Figure 7, we display the total electron heat flux Q_e as a function of the collisional age A_e (see § 4). It can be clearly seen from Figure 7*b* that in the low-pressure and free solar wind, the electron heat flux shows a net upper bound that decreases for an increasing collisional age. However, no significant correlation between Q_e and A_e can be observed (see Fig. 7*a*) when different wind regimes are mixed together. The existence of an upper bound of Q_e as a function of A_e can be hidden by the properties of the compressed regions of the solar wind, characterized by both high heat fluxes and high densities (and thus a high collisional age). Thus, in the ambient solar wind, the maximum observable value of the heat flux decreases when the number of collisions increases. This property strongly suggests that Coulomb collisions play a role in limiting the electron heat flux in the solar wind.

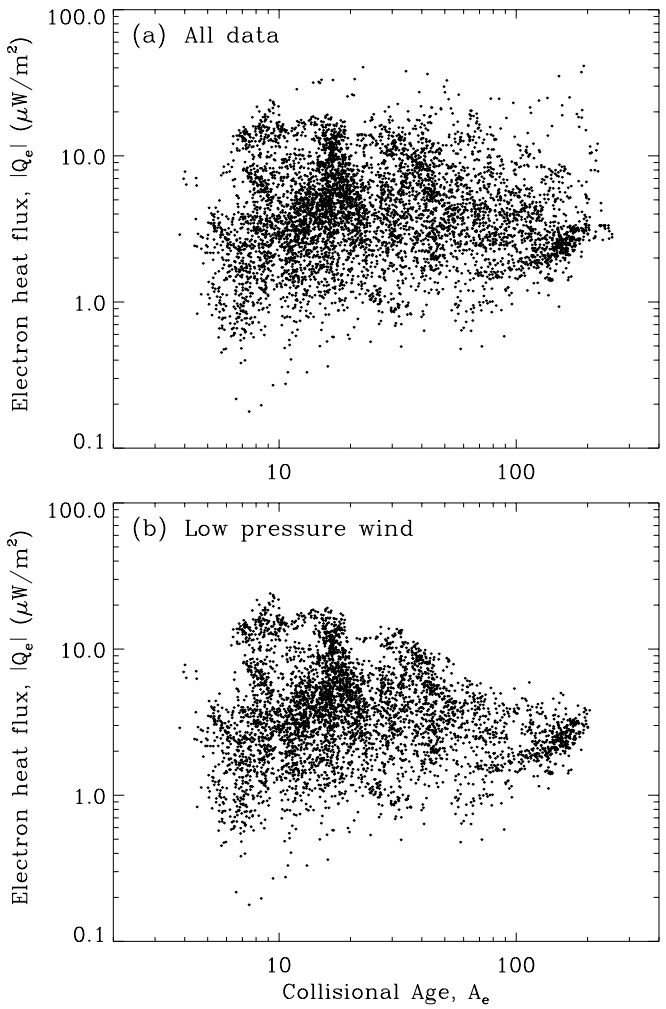

FIG. 7.—Fifty consecutive days. Scatter plots of 11 minute averages of the total electron heat flux Q_e as a function of the collisional age A_e for (*a*) the entire sample in the free solar wind and (*b*) the low-pressure and free solar wind.

5.3. *Comparison with Spitzer-Härm Prediction*

Since the properties of the electron heat flux in the solar wind seem to be partly related to Coulomb collisions between electrons, it is important to understand how the observed heat flux is compared to the classical collisional heat flux of the Spitzer-Härm (SH) theory (Spitzer & Härm 1953). The latter is given by the conventional thermal conductivity equation

$$Q_{e,\mathrm{SH}} = -\kappa_{\parallel} \quad \nabla_{\parallel} T_e \ , \tag{7}$$

where $\kappa_{\parallel}$ is the classical electron thermal conductivity and $\nabla_{\parallel} T_e$ is the temperature gradient, both along the magnetic field. The electron thermal conductivity $\kappa_{\parallel}$ calculated by Spitzer & Härm (1953), taking into account the electron-electron and the electron-proton collisions, is given in MKS units by

$$\kappa_{\parallel} = 3.2 \frac{N_e k_{\mathrm{B}}^2 T_e}{m_e \nu_{ee}} \ , \tag{8}$$

where ν_{ee} is here the basic collisional frequency for transport phenomena (see Spitzer 1956; Huda 2000).

Given the temperature variation with distance, $T_e \propto r^{-\alpha}$, the Spitzer-Härm heat flux at 1 AU can simply be written as

$$Q_{e,\mathrm{SH}} = 0.6 \times 10^{-6} \frac{\alpha T_e^2 N_e}{\nu_{ee}} \ \mu\mathrm{W\ m^{-2}} \ , \tag{9}$$

where T_e is in eV, and N_e in $\mathrm{cm^{-3}}$. In the same units, ν_{ee} can be expressed as (Huda 2000)

$$\nu_{ee} \simeq 2.9 \times 10^{-6} N_e T_e^{-3/2} \ln \Lambda \ , \tag{10}$$

where $\ln \Lambda \simeq 25.5$ (see § 4).

In the previous sections, the collisional properties of the solar wind plasma at 1 AU have been estimated by the collisional age A_e for transverse diffusion (eq. [6]). They can be also estimated by the ratio L_{fp}/L_T between the mean free path L_{fp} of the thermal electrons for transport phenomena and the scale L_T of the temperature gradient. The mean free path L_{fp} of the thermal electrons is conventionally defined as

$$L_{\mathrm{fp}} = v_{\mathrm{the}}/\nu_{ee} \ , \tag{11}$$

where v_{the} is the electron thermal velocity given by equation

(4) and ν_{ee} is given by equation (10). Using the power law $T_e \propto r^{-\alpha}$, the scale L_T of the temperature gradient can be expressed as

$$L_T = \left(\frac{\partial}{\partial r} \ln T_e\right)^{-1} = \frac{R}{\alpha} \tag{12}$$

at the distance of $R = 1$ AU. The smaller the ratio $L_{\rm fp}/L_T$, the higher the collision rate. The advantage of using this parameter instead of the collisional age A_e is that it allows a direct comparison between the observed heat flux and the heat flux predicted by the SH theory. To be exact, we compare here the normalized heat flux Q_n (eq. [2]) and a normalized SH heat flux, $Q_{n,\rm SH}$, i.e., the SH heat flux $Q_{e,\rm SH}$ (eq. [7]) normalized to the free-streaming heat flux Q_0 (eq. [3]) as well. This normalized SH heat flux can then be expressed as a linear function of the ratio $L_{\rm fp}/L_T$,

$$Q_{n,\rm SH} = \frac{Q_{e,\rm SH}}{Q_0} = 1.07 \frac{L_{\rm fp}}{L_T} \ . \tag{13}$$

The comparison is shown in Figure 8. Figure 8*a* displays a scatter plot of Q_n as a function of $L_{\rm fp}/L_T$ for the low-pressure and free solar wind (not compressed and not connected to the Earth's bow shock). Figure 8*b* gives the average value m and the standard deviation σ of the same quantity, in equal bins of $L_{\rm fp}/L_T$: the solid line represents the average m, and the dashed lines represent $m \pm \sigma$, respectively. The solid line labeled SH in both panels represents the normalized SH heat flux of equation (13). There is a tendency for Q_n to be larger when $L_{\rm fp}/L_T$ is large (Fig. 8*b*). Thus, Q_n tends to be larger when there are fewer collisions. This property is another indication that Coulomb collisions play a role in regulating the heat flux.

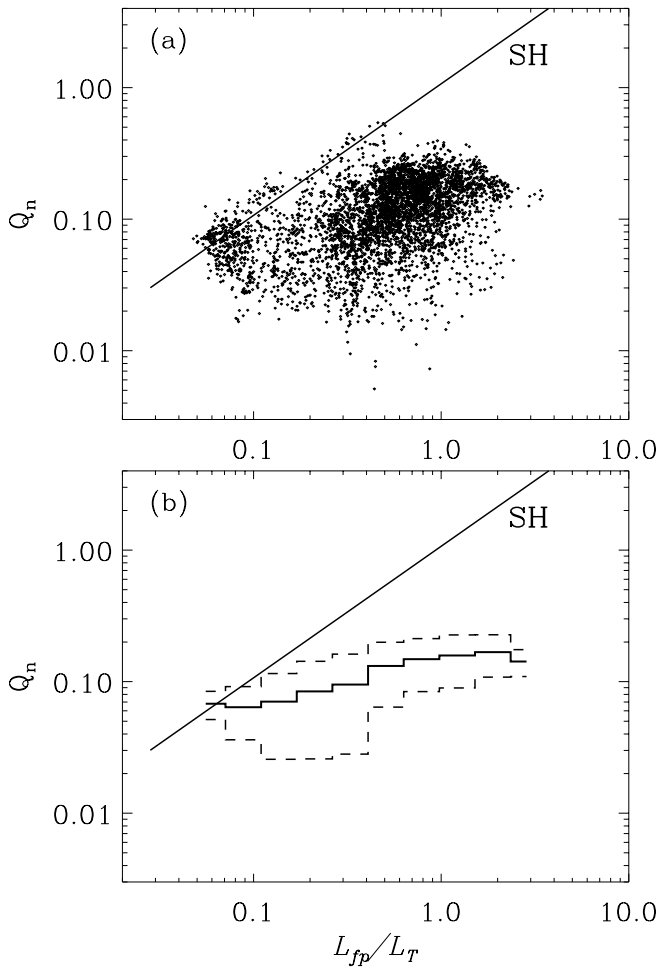

FIG. 8.—Fifty consecutive days. Eleven minute averages of the normalized heat flux Q_n (eq. [2]) in the low-pressure and free (i.e., not connected to the Earth's bow shock) solar wind as a function of the ratio between the electron mean free path $L_{\rm fp}$ (eq. [11]) and the scale of the temperature gradient L_T (eq. [12]). (*a*) Scatter plot. (*b*) Average m (*solid line*) and standard deviation σ ($m \pm \sigma$; *dashed lines*) in equal bins of $L_{\rm fp}/L_T$. The solid line SH in both panels is the normalized heat flux predicted by the classical Spitzer-Härm collisional theory (eq. [13]).

Furthermore, Figure 8 shows another interesting property of the observed heat flux. Although the collisional SH heat flux represents indeed an upper limit to the observed heat flux, it appears that the electron heat flux in the solar wind reaches the SH limit for small values of the ratio $L_{\rm fp}/L_T$, say $L_{\rm fp}/L_T < 0.2$. In contrast, for $L_{\rm fp}/L_T > 0.2$, the observed heat flux is smaller than the SH prediction, as has always been argued (see Scime et al. 1994a). This discrepancy grows stronger as $L_{\rm fp}/L_T$ increases. It is important to note in this respect the differences between the slow and the fast wind, still within the ambient low-pressure solar wind. This can be seen in Figure 9, which displays Q_n as a function of $L_{\rm fp}/L_T$ for a slow solar wind ($V_{\rm sw} < 400$ km s^{-1}; Fig. 9*a*) and for a fast wind ($V_{\rm sw} > 650$ km s^{-1}; Fig. 9*b*). Figure 9*b* shows that the SH limit is not reached within the fast wind where $L_{\rm fp}/L_T$ is usually larger than in the slow wind. In this case, the observed heat flux is nearly 1 order of magnitude below the SH limit.

6. CONCLUSIONS

In this study, we have investigated the properties of solar wind electrons at 1 AU using data from the *Wind* spacecraft, the aim being to determine what physical processes control the electron properties in the solar wind. We examined in particular the nonthermal features of the electron distribution functions, such as temperature anisotropy and heat flux. The question addressed here concerns essentially the role of Coulomb collisions in regulating these nonthermal characteristics. According to different authors, the electron temperature anisotropy $T_{e\parallel}/T_{e\perp}$ in the solar wind mainly appears to depend on the wind speed $V_{\rm sw}$, on the density N_e, on the heliomagnetic latitude λ_m, or on the time. We have shown that $T_{e\parallel}/T_{e\perp}$ actually depends on the collisonal age A_e of the solar wind plasma, i.e., the number of transverse Coulomb collisions suffered by a thermal electron during its travel over the scale (0.5 AU) of the density gradient. A_e depends on $V_{\rm sw}$ and N_e, and thus on λ_m; it depends also on the time, before or after the crossing of the heliospheric current sheet or the SI. The collisional age A_e is thus the physical parameter that controls the temperature anisotropy $T_{e\parallel}/T_{e\perp}$ in the solar wind, but it does not control the electron temperature itself because the energy exchanges due to collisions are much weaker than the momentum exchanges. No correlation has been found between the electron temperature and other solar wind parameters (see also Newbury et al. 1998). The basic mechanisms that regulate the electron temperature in the solar wind are still not understood.

Another indication of the part played by the Coulomb collisions in the solar wind is the value Q_e of the observed heat flux. We have shown the importance of distinguishing between two different wind regimes: the high-pressure

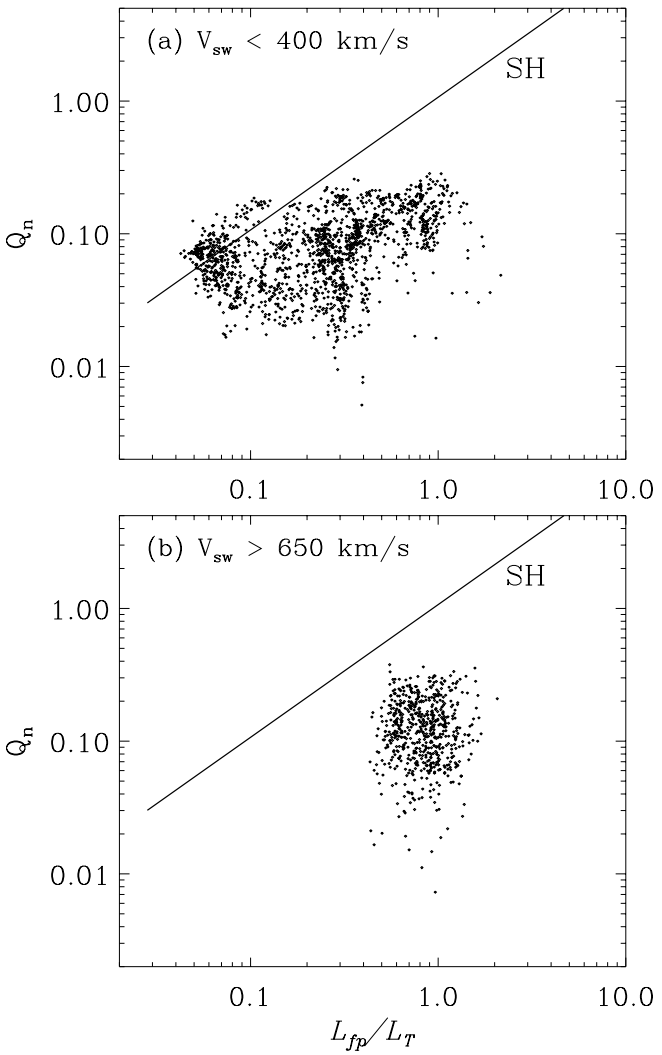

FIG. 9.—Fifty consecutive days. Eleven minute averages of the normalized heat flux Q_n (eq. [2]) as a function of the ratio L_{fp}/L_T, in the low-pressure and free solar wind, for (*a*) a low-speed wind, $V_{sw} < 400$ km s^{-1}, and (*b*) a high-speed wind, $V_{sw} > 650$ km s^{-1}.

compressed wind and the low-pressure ambient wind. These two regions clearly have physical characteristics that are quite different from one another. Using a pressure criterion (see Lacombe et al. 2000), we have selected periods of low-pressure solar wind in order to analyze the properties of the heat flux in the ambient solar wind. We have found that the magnitude of the total heat flux Q_e, in the ambient solar wind, displays an upper bound that tends to decrease with increasing collisional age A_e. Early observations near 1 AU (Montgomery, Bame, & Hundhausen 1968; Hundhausen 1969; Hollweg 1974; Feldman et al. 1975, 1976a, 1976b) and in the inner heliosphere between 0.3 and 1 AU (Pilipp et al. 1987c, 1990) have shown that the electron heat flux is significantly smaller than expected from models of coronal expansion that include a collisional heat flux given by the classical Spitzer-Härm theory (Spitzer & Härm 1953). These observations, as well as more recent observations in and out of ecliptic from *Ulysses* (Scime et al. 1994a, 1999, 2001), led to the conclusion that the electron heat flux must be reduced during the solar wind expansion by an active process other than collisions. However, the relation between the upper bound of the observed heat flux and the number of collisions A_e strongly suggests that the role of Coulomb collisions in regulating the electron heat flux is not as negligible as has always been suggested. We can see here a very good correlation between the electron measurements in the solar wind and what we know about the role of collisions: the more collisions there are, the more the distribution function is isotropized and the smaller is the heat flux. Still, the heat flux due to the Spitzer-Härm electron thermal conductivity represents an upper limit to the observed heat flux, but we have shown that this limit is reached for electron mean free paths L_{fp} normalized to the scale of the temperature gradient L_T, L_{fp}/L_T of about 0.06–0.15. For $L_{fp}/L_T > 0.2$, the deviation of the observations from the SH prediction grows with the parameter L_{fp}/L_T. This deviation is highest in the high-speed solar wind streams characterized by larger mean free paths. Actually, the approximate solution of the Fokker-Planck equation used by Spitzer & Härm (1953) in their calculation of the heat flux is based on a model with a heat flux carried by a small perturbation to a local Maxwellian particle distribution function. This implies a collisional mean free path L_{fp} much smaller than the scale L_T of the temperature gradient. According to Bell, Evans, & Nicholas (1981) and/or Campbell (1984), this determination of the heat flux is not valid for $L_{fp}/L_T > 10^{-3}$; meanwhile, in the solar wind at 1 AU, L_{fp}/L_T is found to lie between 0.04 and 1. Another model of the classical collisional heat flux, extending Spitzer's calculation to large temperature gradients, could provide predictions closer to the observed values. A different class of solutions to the Fokker-Planck equation are required to determine the thermal conductivity where the plasma is far from local thermodynamic equilibrium.

In other interpretations (see Scime et al. 1994a; Gary et al. 1994, 1999), the heat flux is not regulated by collisions but by wave-particle interactions. Such wave-particle interactions, due to some instability growth, thermalize the electrons carrying the bulk of the electron heat flux by scattering them in the core electron population. In these interpretations, the upper bound of the observed heat flux is related to the threshold of a heat flux instability. As argued by Marsch (1991), both processes, Coulomb collisions and wave-particle interactions, are most likely to play roles in determining solar wind electron dynamics. Therefore, it is necessary to understand their individual contributions to thermal conduction in the solar wind. New *Wind* observations with respect to the possibility of a heat flux regulation by wave-particle interactions will be presented in a forthcoming paper.

The 3D Plasma experiment (PI: R. P. Lin) on *Wind* is a joint effort of the Space Sciences Laboratory (Berkeley), the University of Washington, the CESR (Toulouse, France), ESTEC (the Netherlands), and the Max-Planck-Institut (Germany). The Waves instrument (whose PI is now M. L. Kaiser) was built by teams at the Paris-Meudon Observatory, the University of Minnesota, the University of Iowa, and the Goddard Space Flight Center. Use of the *Wind* spin resolution MFI data and SWE data is courtesy of the teams of the Magnetic Field Investigation experiment (PI: R. P. Lepping). Work at UC Berkeley is supported by NASA grant FDNAG5-11804 to the University of California.

REFERENCES

Bell, A. R., Evans, R. G., & Nicholas, D. J. 1981, Phys. Rev. Lett., 46, 243
Borrini, G., Gosling, J. T., Bame, S. J., Feldman, W. C., & Wilcox, J. M. 1981, J. Geophys. Res., 86, 4565
Bougeret, J.-L., et al. 1995, Space Sci. Rev., 71, 231
Bruno, R., Villante, U., Bavassano, B., Schwenn, R., & Mariani, F. 1986, Sol. Phys., 104, 431
Campbell, P. M. 1984, Phys. Rev. A, 30, 365
David, C., Gabriel, A. H., Bely-Dubau, F., Fludra, A., Lemaire, P., & Wilhelm, K. 1998, A&A, 336, L90
Feldman, W. C., Asbridge, J. R., Bame, S. J., Gary, S. P., & Montgomery, M. D. 1976a, J. Geophys. Res., 81, 2377
Feldman, W. C., Asbridge, J. R., Bame, S. J., Gary, S. P., Montgomery, M. D., & Zink, S. M. 1976b, J. Geophys. Res., 81, 5207
Feldman, W. C., Asbridge, J. R., Bame, S. J., Montgomery, M. D., & Gary, S. P. 1975, J. Geophys. Res., 80, 4181
Fitzenreiter, R. J., Ogilvie, K. W., Chornay, D. J., & Keller, J. 1998, Geophys. Res. Lett., 25, 249
Fludra, A., Del Zanna, G., Alexander, D., & Bromage, B. J. I. 1999, J. Geophys. Res., 104, 9709
Gary, S. P., Scime, E. E., Phillips, J. L., & Feldman, W. C. 1994, J. Geophys. Res., 99, 23391
Gary, S. P., Skoug, R. M., & Daughton, W. 1999, Phys. Plasmas, 6, 2607
Gibson, S. E., Fludra, A., Bagenal, F., Biesecker, D., del Zanna, G., & Bromage, B. 1999, J. Geophys. Res., 104, 9691
Gosling, J. T., Asbridge, J. R., Bame, S. J., & Feldman, W. C. 1978, J. Geophys. Res., 83, 1401
Hammond, C. M., Feldman, W. C., McComas, D. J., Phillips, J. L., & Forsyth, R. J. 1996, A&A, 316, 350
Hoeksema, J. T., Wilcox, J. M., & Scherrer, P. H. 1983, J. Geophys. Res., 88, 9910
Hollweg, J. V. 1974, J. Geophys. Res., 79, 3845
Huda, J. D. 2000, NRL Plasma Formulary (Washington, DC: Naval Res. Lab.)
Hundhausen, A. J. 1969, J. Geophys. Res., 74, 5810
———. 1972, Coronal Expansion and Solar Wind (Berlin: Springer)
Issautier, K., Meyer-Vernet, N., Moncuquet, M., & Hoang, S. 1998, J. Geophys. Res., 103, 1969
Issautier, K., Meyer-Vernet, N., Moncuquet, M., Hoang, S., & McComas, D. J. 1999, J. Geophys. Res., 104, 6691
Jockers, K. 1970, A&A, 6, 219
Lacombe, C., Salem, C., Mangeney, A., Hubert, D., Perche, C., Bougeret, J.-L., Kellogg, P. J., & Bosqued, J.-M. 2002, Ann. Geophys., 20, 609
Lacombe, C., Salem, C., Mangeney, A., Steinberg, J.-L., Maksimovic, M., & Bosqued, J.-M. 2000, Ann. Geophys., 18, 852
Lemaire, J., & Scherer, M. 1971, J. Geophys. Res., 76, 7479
Lepping, R. P., et al. 1995, Space Sci. Rev., 71, 207
Lin, R. P., et al. 1995, Space Sci. Rev., 71, 125
Maksimovic, M., Gary, S. P., & Skoug, R. M. 2000, J. Geophys. Res., 105, 18337
Maksimovic, M., Pierrard, V., & Lemaire, J. F. 1997, A&A, 324, 725
Mangeney, A., et al. 1999, Ann. Geophys., 17, 307
Marsch, E. 1991, in Physics of the Inner Heliosphere II. Particles, Waves and Turbulence, ed. R. Schwenn & E. Marsch (New York: Springer), 45
Meyer-Vernet, N. 1999, European J. Phys., 20, 167
Meyer-Vernet, N., Hoang, S., Issautier, K., Maksimovic, M., Manning, R., Moncuquet, M., & Stone, R. G. 1998, in Measurement Techniques for Space Plasma: Fields, ed. R. F. Pfaff et al. (Geophys. Monogr. 103; Washington, DC: AGU), 205
Montgomery, M. D., Bame, S. J., & Hundhausen, A. J. 1968, J. Geophys. Res., 73, 4999
Newbury, J. A., Russell, C. T., Phillips, J. L., & Gary, S. P. 1998, J. Geophys. Res., 103, 9553
Ogilvie, K. W., Burlaga, L. F., Chornay, D. J., & Fitzenreiter, R. J. 1999, J. Geophys. Res., 104, 22389
Parker, E. N. 1964, ApJ, 139, 93
Phillips, J. L., Bame, S. J., Gary, S. P., Gosling, J. T., Scime, E. E., & Forsyth, R. J. 1995, Space Sci. Rev., 72, 109
Phillips, J. L., & Gosling, J. T. 1990, J. Geophys. Res., 95, 4217
Phillips, J. L., Gosling, J. T., McComas, D. J., Bame, S. J., Gary, S. P., & Smith, E. J. 1989, J. Geophys. Res., 94, 6563
Pilipp, W. G., Miggenrieder, H., Montgomery, M. D., Mühlhäuser, K.-H., Rosenbauer, H., & Schwenn, R. 1987a, J. Geophys. Res., 92, 1075
———. 1987b, J. Geophys. Res., 92, 1093
Pilipp, W. G., Miggenrieder, H., Mühlhäuser, K.-H., Rosenbauer, H., & Schwenn, R. 1990, J. Geophys. Res., 95, 6305
Pilipp, W. G., Miggenrieder, H., Mühlhäuser, K.-H., Rosenbauer, H., Schwenn, R., & Neubauer, F. M. 1987c, J. Geophys. Res., 92, 1103
Pizzo, V. J. 1994, J. Geophys. Res., 99, 4185
Salem, C. 2000, Ph.D. thesis, Univ. Paris
Salem, C., Bosqued, J.-M., Larson, D. E., Mangeney, A., Maksimovic, M., Perche, C., Lin, R. P., & Bougeret, J.-L. 2001, J. Geophys. Res., 106, 21710
Sanderson, T. R., et al. 1998, J. Geophys. Res., 103, 17235
Scime, E. E., Badeau, A. E., & Littleton, J. E. 1999, Geophys. Res. Lett., 26, 2129
Scime, E. E., Bame, S. J., Feldman, W. C., Gary, S. P., Phillips, J. L., & Balogh, A. 1994a, J. Geophys. Res., 99, 23401
Scime, E. E., Bame, S. J., Phillips, J. L., & Balogh, A. 1995, Space Sci. Rev., 72, 105
Scime, E. E., Littleton, J. E., Gary, S. P., Skoug, R., & Lin, N. 2001, Geophys. Res. Lett., 28, 2169
Scime, E. E., Phillips, J. L., & Bame, S. J. 1994b, J. Geophys. Res., 99, 14769
Scudder, J. D., & Olbert, S. 1979a, J. Geophys. Res., 84, 2755
———. 1979b, J. Geophys. Res., 84 A, 6603
Song, P., Zhang, X. X., & Paschmann, G. 1997, Planet. Space Sci., 45, 255
Spitzer, L. 1956, Physics of Fully Ionized Gases (New York: Interscience)
Spitzer, L., & Härm, R. 1953, Phys. Rev., 98, 977